ADVANCED FUNCTIONAL MATERIALS
www.afm-journal.de

High-Performance Phototransistors Based on Organic Microribbons Prepared by a Solution Self-Assembly Process

By *Yunlong Guo, Chunyan Du, Gui Yu,* Chong-an Di, Shidong Jiang, Hongxia Xi, Jian Zheng, Shouke Yan, Cailan Yu, Wenping Hu,* and *Yunqi Liu**

Oligoarenes as an alternative group of promising semiconductors in organic optoelectronics have attracted much attention. However, high-performance and low-cost opto-electrical devices based on linear asymmetric oligoarenes with nano/microstructures are still rarely studied because of difficulties both in synthesis and high-quality nano/microstructure growth. Here, a novel linear asymmetric oligoarene 6-methyl-anthra[2,3-*b*]benzo[*d*]thiophene (Me-ABT) is synthesized and its high-quality microribbons are grown by a solution process. The solution of Me-ABT exhibits a moderate fluorescence quantum yield of 0.34, while the microribbons show a glaucous light emission. Phototransistors based on an individual Me-ABT microribbon prepared by a solution-phase self-assembly process showed a high mobility of 1.66 $cm^2 V^{-1} s^{-1}$, a large photoresponsivity of 12 000 A W^{-1}, and a photocurrent/dark-current ratio of 6000 even under low light power conditions (30 $\mu W\ cm^{-2}$). The measured photoresponsivity of the devices is much higher than that of inorganic single-crystal silicon thin film transistors. These studies should boost the development of the organic semiconductors with high-quality microstructures for potential application in organic optoelectronics.

1. Introduction

Organic nano/microstructure semiconductors have undergone great development in the past decade because of their merits in studying intrinsic properties, their high-performance and promising applications in low-cost microelectronics, such as active matrix displays, phototransistors, memory arrays, organic lasers, solar cells, and gas sensors.[1–4] From the point of nano/microstructure growth, physical vapor transport techniques (PVTs) and solution process are the two major ways to obtain quality nano/microstructures. However, in previous works, most of the progress and attention has focussed on high-performance device fabrication based on PVT due to the higher quality nano/microstructure growth. Only recently have various devices based on nano/microstructures grown from solution been developed greatly.[1c,5–8] Among these devices, organic nano/microstructure phototransistors (ON/MPTs) as one of the functional devices that integrate the switching ability of a transistor with light detection, have attracted many researchers' attention.[2] However, synthetic materials with comprehensively excellent properties and high-quality nano/microstructures for ON/MPTs obtained by a solution process are still limited. Furthermore, the mechanism of high-performance ON/MPTs is not well understood, and it is important to guide the material synthesis and device fabrication.

The synthesis of organic semiconducting materials is a key driving force for the development of organic electronics. In previous reports, the symmetric oligoarenes have been an important part of synthetic organic semiconductors. Only recently, asymmetric oligoarenes as an alternative group of promising materials have attracted considerable attention because of their unique molecular structures and excellent electronic properties.[9] However, there are few reports on the intrinsic opto-electrical behavior of the asymmetric oligoarenes because of the complicated synthesis and the difficulty in crystal growth. Correspondingly, the exploration of the optical and electrical properties of asymmetric oligoarenes based on high-quality nano/microstructures prepared by a low-cost process could be an alternative way to further discern the intrinsic properties of these materials. Therefore, the search for new asymmetric organic semiconductors and growth of high-quality microstructures with novel opto-electrical properties by a low-cost solution process are highly desired for the development of the organic semiconductors.

In this study, we present a linear asymmetric oligoarene, 6-methyl-anthra[2,3-*b*]benzo[*d*]thiophene (Me-ABT) with excellent opto-electrical properties. Moreover, we fabricated organic phototransistors (OPTs) based on an individual Me-ABT microribbon utilizing the solution assembly process. The organic microribbon

[*] Prof. Y. Liu, Prof. G. Yu, Y. Guo, C. Du, Dr. C.-a. Di, Dr. S. Jiang, H. Xi, J. Zheng, Prof. S. Yan, C. Yu, Prof. W. Hu
Beijing National Laboratory for Molecular Sciences
Institute of Chemistry
Chinese Academy of Sciences
Beijing 100190 (P. R. China)
E-mail: yugui@iccas.ac.cn; liuyq@iccas.ac.cn
Y. Guo, C. Du, H. Xi, J. Zheng
Graduate School of Chinese Academy of sciences
Beijing 100049 (P. R. China)

DOI: 10.1002/adfm.200901662

phototransistor (OMPT) exhibits a high light sensitivity with a responsivity (R) of 12 000 A W^{-1}, a photocurrent/dark-current ratio (P) of 6000, and a hole mobility of 1.66 cm^2 V^{-1} s^{-1}. For comparison, thin film OPTs were also fabricated by vacuum deposition and show a moderate light sensitivity with a responsivity (R) of 447 A W^{-1}, a photocurrent/dark-current ratio (P) of 4000, and a hole mobility of 0.18 cm^2 V^{-1} s^{-1}. Furthermore, the mechanism was also analyzed on OPTs with different condensed states of Me-ABT (i.e., thin film and microribbon) to explore the origin of the high device performance.

2. Results and Discussion

The compound Me-ABT was synthesized according to Scheme 1 and purified by repeated sublimation after recrystallization. Notably, considering the structure of 4-methyl-phthalic anhydride, the reactions of the Friedel–Crafts acylation may induce two possible isomers (**1a** and **1b**), as illustrated by Scheme 1. Since the elemental analysis and mass spectrometry of the product exclude the presence of significant amounts of chemical impurities, the multipeaks and complicated adjacent H interactions in the ^{1}H NMR, NOESY and COSY NMR spectra have proved the presence of the isomer (see Fig. S1−S3). According to the mechanism of Friedel–Crafts acylation, we assigned compound **1a** to be the main product. In practice, however, this separation of the different isomer fractions was often found to be difficult because of the rather small differences of sublimation temperature. So the compound here is investigated as a mixture of Me-ABTa and Me-ABTb, and to ease the complication of the article, we only refer to the sample as Me-ABT and draw it as the structure of Me-ABTa. The sample used was purified by using a three-zone furnace sublimation three times. The physical properties of Me-ABT were characterized by thermogravimetric analysis (TGA), UV-vis absorption spectroscopy, and cyclic voltammetry (CV). No decomposition was observed for Me-ABT until about 300 °C, which suggests a good thermal stability of the compound (Fig. 1A). Although the Me-ABT has a molecular structure similar to that of pentacene, it is quite soluble in common non-polar organic solvents, for example, toluene and chloroform. On the other hand, the Me-ABT molecule becomes insoluble in more-polar solvents such as alcohol and methanol.

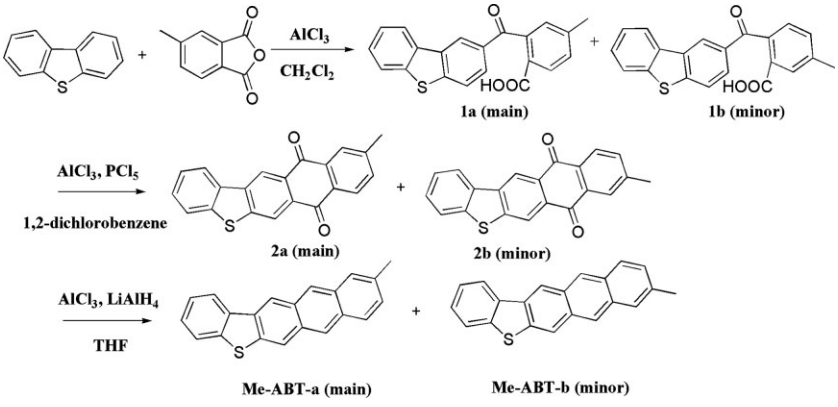

Scheme 1. The synthesis of Me-ABT.

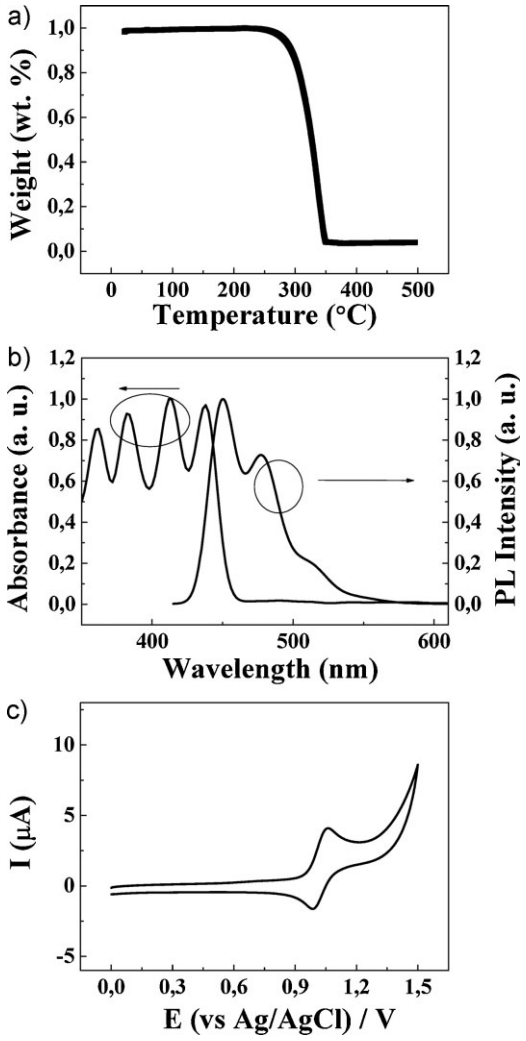

Figure 1. a) TGA plots of Me-ABT with a heating rate of 10 °C min^{-1} under N_2. b) The absorption and PL spectra of the Me-ABT in dichloromethane. c) Cyclic voltammogram of the compound Me-ABT.

The absorption spectrum of Me-ABT in dichloromethane shows a maximum peak at 437 nm (Fig. 1B). The optical bandgap of Me-ABT is 2.76 eV determined by extrapolating the long-wavelength absorption edge. The oxidation potential of Me-ABT was studied by CV measurements (Fig. 1C). The Me-ABT exhibits reversible oxidation waves with a half-oxidation potential of 1.02–1.07 eV and an onset oxidation potential of 0.94 eV. The energy levels of the highest occupied molecular orbitals were estimated from the onset oxidation potential to be around −5.34 eV, which matches well with the work function of gold metal (−5.2 eV).[8d] This datum is lower than that observed for pentacene and most oligothiophenes, which indicates better environmental stability. The fluorescence quantum yield of Me-ABT in dichloromethane was measured to be 0.34 by using 9,10-diphenylanthracene as a standard.

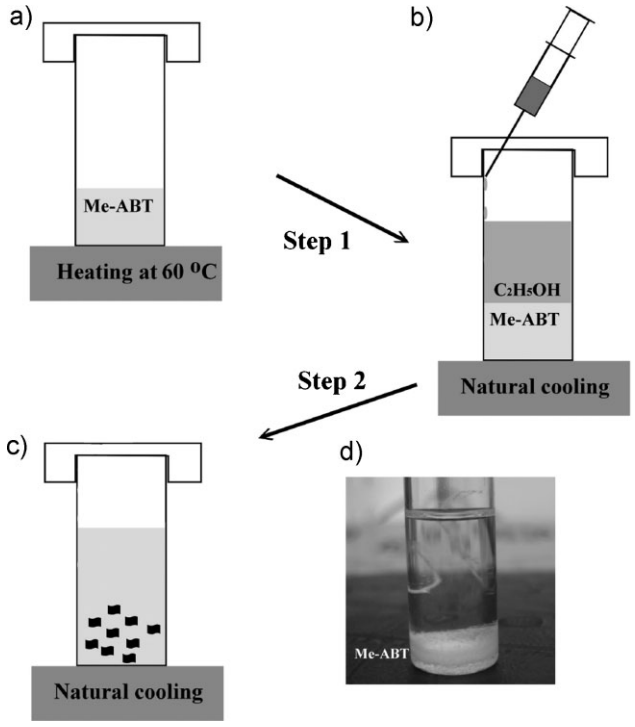

Figure 2. Microstructure self-assembly process of the Me-ABT molecules through the solvent exchange method in the solution phase. a) Heating at 60 °C to dissolve Me-ABT in chloroform and obtain its saturated solution. b) Injection of ethanol into the solution. c) Precipitation of the Me-ABT microribbons from chloroform/ethanol solution. d) A photograph of the solution with the Me-ABT microstuctures.

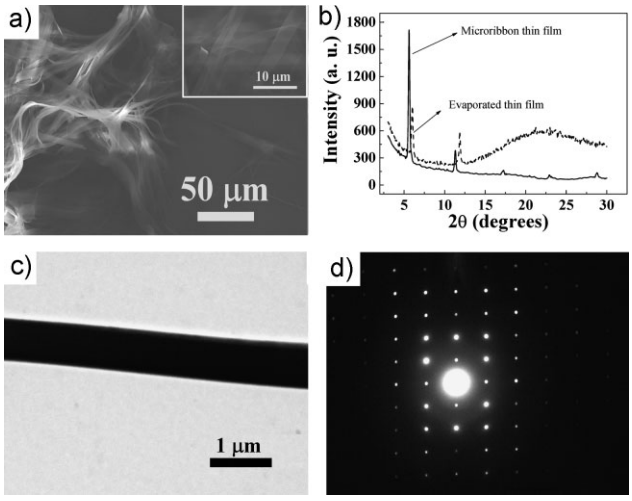

Figure 3. a) SEM image of the Me-ABT microstructure assemblies. b) The XRD data of the large area Me-ABT microribbons on the silicon substrate and the evaporated thin films on OTS-treated SiO_2 substrate. c) TEM image of a Me-ABT microribbon, and d) its corresponding selected area electron diffraction pattern.

The Me-ABT microstructures were prepared from the powder as the starting material by a solvent-exchange method in the solution phase (Fig. 2). A saturated solution of the Me-ABT in chloroform (about 1 mL) was injected into a closed chamber at 60 °C. The heating was stopped and 2 mL of ethanol was added into the chamber to lead to the self-assembly of the Me-ABT molecules. The assembled catkin-like product was suspended at the surface of the chloroform/ethanol (see Fig. 2D). The Me-ABT easily self-assembles into microribbons with a width of 1–8 μm and a length of hundreds of micrometers (see Fig. 3A). The X-ray diffraction (XRD) measurement was performed on the Me-ABT evaporated and microribbon thin films (see Fig. 3B). The microribbon thin films show serial high-ordered diffraction peaks at 2θ values of 5.620°, 11.339°, 17.261°, 22.902°, and 28.801°, which indicates that microribbons in a large area have a high crystallinity. However, the evaporated thin films show a less ordered structure with two diffraction peaks at 2θ of 5.620° and 11.810°. In fact, the twist microribbons were found in scanning electron microscopy (SEM) images of the Me-ABT product and still can be bent by a machine probe, which demonstrates their excellent flexibility. It is clear to see that an individual ribbon with a length of about 1000 μm was bent like a 'C' shape, which may demonstrate a potential application in flexible electronics (see Fig. S4). Although both Me-ABTa and Me-ABTb exist in the powder product, surprisingly, a high-quality microribbon can still be obtained. Figure 3C shows the transmission electron microscopy (TEM) image of a representative Me-ABT microribbon, and Figure 3D shows the selected area electron diffraction (SAED) pattern obtained from the same microribbon, which demonstrated the high quality of the ribbons. The optical image of the microribbons with glaucous emission was shown in Fig. S5A. The fluorescence spectrum of the Me-ABT microribbons on the quartz substrate are shown in Figure S5B with a maximum peak at 494 nm.

Top-contact OMPTs were fabricated using an individual Me-ABT microribbon precipitated from chloroform/alcohol solution. A heavily doped n-type Si substrate and a 500 nm SiO_2 layer with a capacitance per unit area of 7.5 nF cm^{-2} were used as a gate electrode and gate dielectric layer, respectively. The microribbon was dropped on the *n*-octadecyltrimethoxysilane (OTS)-treated SiO_2/Si substrate. Gold shadow masks were used to deposit the gold source/drain electrodes. A typical schematic diagram of the device is shown in Figure 4A. An optical image of the microribbon device is shown in Figure 4B. The microribbon with a width of 2 μm and a thickness of 80 nm was characterized by atomic force microscopy (AFM) (see inset of Fig. 4B). The electrical characteristics of transistors based on individual Me-ABT microribbons are shown in Figure 4C and D. The mobility of the OMPTs in the saturation region was extracted from the following equation:

$$I_{DS} = \frac{W}{2L}\mu C_i(V_{GS} - V_{th})^2 \quad (1)$$

where I_{DS} is the source–drain current, μ is the field-effect mobility, C_i is the capacitance per unit area of the gate dielectric layer, V_{GS} is the gate voltage, V_{th} is the threshold voltage, and L and W are the channel length and width, respectively. The V_{th} of the device was determined by extrapolating the $(|I_{DS,sat}|)^{1/2}$ vs V_{GS} plot to $I_{DS} = 0$. The transistors exhibit a p-channel behavior with a highest μ of 1.66 cm^2 V^{-1} s^{-1} estimated from the saturation current, a V_{th} of −10 V, and a high on/off ratio of 10^6, which is one

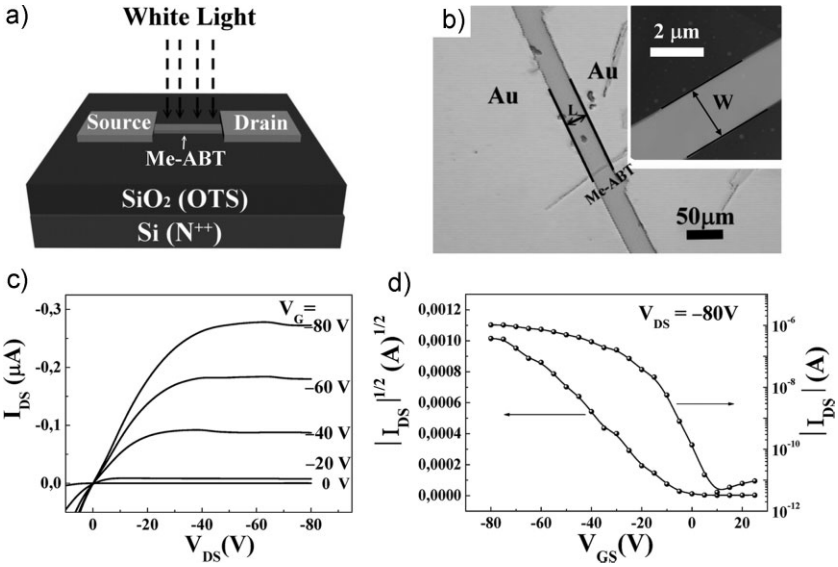

Figure 4. Field-effect characteristics of OFETs based on an individual Me-ABT microribbon. a) Schematic diagram of the microribbon phototransistor. b) The microscope image of the OFET based on the individual Me-ABT microribbon. Inset is the corresponding AFM image. c) Output and d) transfer characteristics.

of the best results for a microribbon transistor formed by a solution process. In previous reports, the performance of devices was always affected by the thickness of the microribbons.[2a,3a] Therefore, devices based on Me-ABT microribbons with different thickness were fabricated and the mobilities ranged from 0.34 to 1.66 $cm^2\ V^{-1}\ s^{-1}$, with an average value of 0.85 $cm^2\ V^{-1}\ s^{-1}$ (see Fig. 5A), which demonstrated that our microribbon is thin enough (most thicknesses lower than 100 nm) to fabricate high performance transistors. The on/off current cycle test was performed on one representative device and a good stability was shown over 1000 test cycles (see Fig. 5B).

For inorganic and organic phototransistors, the mobility, light responsivity (R), and photocurrent/dark-current ratio (P) are three key parameters. The R is defined by the following equation:[11]

$$R = \frac{I_{ph}}{P_{ill}} = \frac{I_l - I_{dark}}{P_{ill}} \quad (2)$$

where I_{ph} is the photocurrent, P_{ill} the incident illumination power on the channel of the device, I_l the drain current under illumination, and I_{dark} the drain current in the dark. The responsivity reveals to what extend the optical power is converted into an electrical current. The other merit is the photocurrent/dark-current ratio (P):

$$P = \frac{\text{signal}}{\text{noise}} = \frac{I_{ph}}{I_d} = \frac{I_l - I_{dark}}{I_{dark}} \quad (3)$$

where all terms have been previous defined. Here, the I–V characteristics of the transfer curve based on the OMPT shows a large change, even under 30 $\mu W\ cm^{-2}$ low-power condition. The transistor exhibits a high mobility of 1.66 $cm^2\ V^{-1}\ s^{-1}$ at the saturation area. The OMPT shows high light sensitivity with a R value of 12 000 A W^{-1} and with a P value of 6000 at the cross point of the two curves with $V_{DS} = -80$ V and $V_{GS} = -18$ V (see Fig. 6A and B). The measured photosensitivity of the devices is much higher than that of inorganic single-crystal silicon thin film transistors (300 A W^{-1}).[12] To the best of our knowledge, the result obtained here is one of the highest value of photosensitivity for OPTs. On the other hand, we also fabricated OPTs based on the Me-ABT thin film. Compared with the microribbon devices, the Me-ABT thin film transistors exhibit a lower mobility of 0.18 $cm^2\ V^{-1}\ s^{-1}$ at a deposit substrate temperature of 40 °C (output and transfer curves, see Fig. S6A and B), a lower light sensitivity R of 477 A W^{-1}, and a smaller P of 4000 at the cross point of the two curves with $V_{DS} = -100$ V and $V_{GS} = 12$ V (see Fig. S6C and D). The mobility and R values obtained are lower than those of our previous reported thin film phototransistors based on anthra[2,3-*b*]benzo[*d*]thiophene (ABT) with a mobility of 0.40 $cm^2\ V^{-1}\ s^{-1}$ and R of 1000 A W^{-1},[2h] but the R and P values are still higher than those of OPTs based on

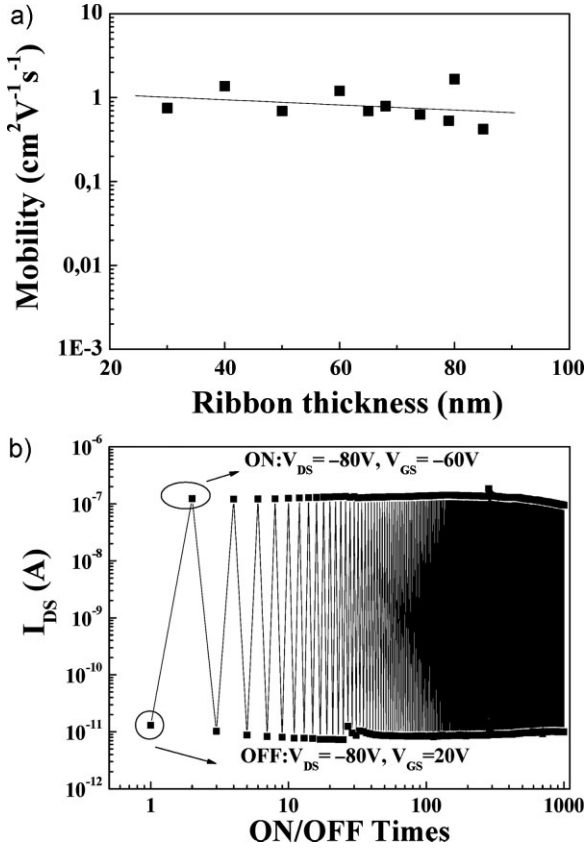

Figure 5. a) Field-effect mobility of the Me-ABT microribbon transistors plotted as a function of the ribbon thickness. b) The on/off current cycle testing of one representative device.

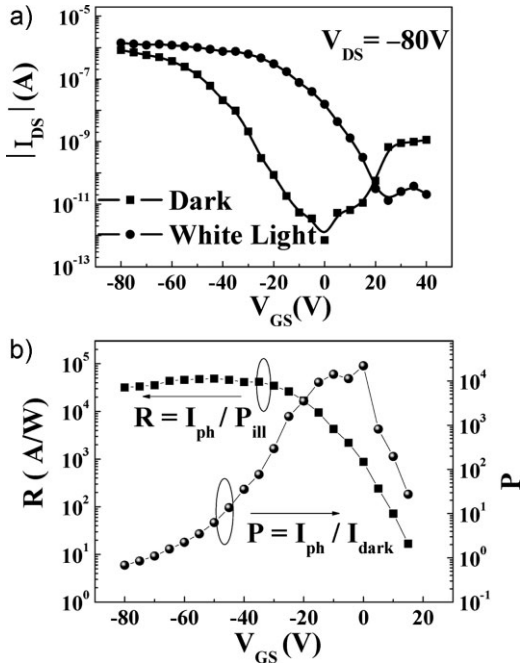

Figure 6. a) The transfer characteristics of OMPTs based on an individual Me-ABT microribbon in the dark and under white light irradiation with a low power of 30 μW cm^{-2}. b) Responsivity (*R*) and photocurrent/dark-current ratio (*P*) versus V_{GS} behavior for the OMPT.

pentacene or tetracene.[10] Although the exact mechanism for the highly sensitive phenomenon of our devices is not precisely understood, we propose a possible mechanism and analyze it based on the following two aspects. First, the intrinsic property of the Me-ABT is the main factor, i.e., the moderate quantum yield of 0.34, that determines the exciton-yield quality and numbers under the same conditions (i.e., with same light power and wavelength).[2f] Second, the life-time of excitons demonstrate excitons with enough time to be separated into free charges by the vertical V_{GS} and the parallel V_{DS}, which is an important factor to improve the performance of OPTs.[10] The fluorescence decay of the Me-ABT microribbons was measured by an Edinburgh Analytical Instruments-FLS920 and the life-time of excitons was between 0.7 and 5 ns (see Fig. S7), which is higher than that of pentacene (~1 ps) and tetracene (~0.2 ns).[10]

The high-quality microstructure has less disorder and grain boundaries than the thin films. Correspondingly, the OMPTs could show higher carrier mobility and higher light sensitivity than those of the thin films.[2a,2i] For this phenomenon, we performed an analysis based on Me-ABT. Different condensed states of Me-ABT such as a thin-film and a microribbon own different degrees of ordered molecular packing. The XRD data shows more ordered molecular packing in microribbons than thin film ones, which may demonstrate the higher mobility of the microribbons.[2] Meanwhile, high ordered molecular packing has also provided a higher velocity conducting-channel for the separated charges. Furthermore, the exciton dissociation in a disordered thin film is inefficient because of recombination at the disordered area and dissipation.[2a] Therefore, for OPTs with the same organic semiconductor material, the higher ordered condensed states will impart a higher I_l with the same light conditions and almost the same I_{dark}. According to Equation (2), you will then obtain a higher *R* value. For the Me-ABT OPTs with the same light absorbance and electrodes for collection (with same *S*–*D* material), the condensed states with efficient exiton dissociation, exiton separation, and fast travelling of free charges, will achieve a higher *R* value. That is to say, the performance of OMPTs is higher than that of the thin-film phototransistors based on Me-ABT, which is consistent with the previous report of F_{16}CuPc.[2a,2i]

3. Conclusions

A novel organic semiconductor, Me-ABT, which easily self-assembles to form high-quality microribbons, is synthesized. The OMPTs were fabricated based on individual microribbons prepared by a solution-phase self-assembly process. The OMPTs showed a large mobility, high *R*, and *P* values. Furthermore, the mechanism of the OPTs fabrication was analyzed for different Me-ABT condensed states. All these studies should boost the development of the asymmetric organic semiconductors with microstructures for potential application in the high-performance and low-energy exhaust organic optoelectronics.

4. Experimental

Instrumentation: Elemental analyses were obtained with a Carlo Erba model 1160 elemental analyzer. Mass spectra were obtained on a Micromass GCT-MS spectrometer. The ^{1}H NMR spectra were measured on a Bruker DMX-300 NMR spectrometer using tetramethylsilane as an internal standard. The photoluminescence (PL) and absorption spectra were measured on an F-4500 fluorescence spectrophotometer and a U-3010 UV-vis spectrophotometer, respectively. Cyclic voltammetric measurements were carried out on a computer-controlled CHI660C instrument at room temperature with CH_2Cl_2 as solvent, 0.1 M Bu_4NPF_4 as a supporting electrode, and Ag/AgCl electrode as a referring electrode. TGA was performed on a TA SDT 2960 thermogravimeter under a dry nitrogen gas flow at a heating rate of 10 °C min^{-1}. The XRD of thin films was obtained in the reflection mode at 40 kV and 200 mA with Cu Kα radiation using a 2 kW Rigaku X-ray diffractometer. Fluorescence microscopy was performed on an Olympus IX 71. An SEM image was measured on a Hitachi S-4300 field emission scanning electron microscope. The fluorescence decay was measured by the Edinburgh Analytical Instruments-FLS920. TEM images were obtained on a Hitachi H-800 transmission electron microscope. AFM images were determined with a Nanoscope IIIa AFM (Digital Instruments) in tapping mode.

Device Preparation and Characterization: The thin film transistors were fabricated with a top contact configuration. The substrate, gate electrode, insulator and its modified layer are all the same as for OMPT using OTS-treated SiO_2/Si substrate with a heavily N-doped Si gate electrode. The Me-ABT thin films were thermally evaporated under a vacuum pressure of 2×10^{-4} Pa. Shadow masks with a length of 50 μm and a width of 3 mm were used to deposit the gold source–drain (*S*–*D*) electrodes. The electrical characteristics of the devices were measured with a Keithley 4200 SCS semiconductor parameter analyzer under ambient conditions at room temperature.

Synthetic Procedures of the Compounds: Here we only list the ^{1}H NMR of the main products.

1) 2-(3-Methyl-2-carboxybenzoyl)dibenzothiophene (**1**): A suspension of 4-methyl-phthalic anhydride (1.7 g, 10.5 mmol) in 20 mL of dichloromethane was added to a solution of aluminum chloride (4 g) in dichloromethane (100 mL). After the addition was complete, the reaction mixture was stirred for 30 min, and then dibenzothiophene (2 g, 11 mmol)

was added dropwise into the reaction mixture under cooling with ice. The reaction mixture was stirred for 4 h at room temperature, and then was poured into a solution of water (100 mL) and concentrated hydrochloric acid (40 mL). The organic layers were separated and dried. The solvents were removed under a reduced pressure. The product was purified by recrystallization from ethanol to provide an orange solid (2.9 g, 80%). ^{1}H NMR (400 MHz, $CDCl_3$, δ): 2.34 (s, 3H), 7.50–7.52 (m, 2H), 7.67–7.71 (m, 2H), 7.87 (s, 1H), 7.98–8.02 (m, 2H), 8.08 (s, 1H), 8.27 (s, 1H), 8.55 (s, 1H), 11.55 (s, 1H). EIMS (m/z): 346 (M^+) (Calcd. for $C_{21}H_{14}O_3S$: 346.1).

2) 6-Methyl-9,10-dione-anthra[2,3-*b*]benzo[*d*]thiophene (**2**): To 20 mL of dry 1,2-dichlorobenzene was added compound **1** (2 g, 5.8 mmol) and PCl_5 (1.8 g, 8.6 mmol), and $AlCl_3$ (1.15 g, 8.6 mmol). After the reaction mixture was heated at 140 °C for 12 h, the solution was cooled to room temperature. The solvents were removed under a reduced pressure. The crude product was purified by column chromatography on silica gel using toluene as eluent to give a yellow green solid (1.3 g, 68.6%). ^{1}H NMR (400 MHz, $CDCl_3$, δ): 2.34 (s, 3H), 7.50–7.52 (m, 3H), 7.59 (s, 1H), 7.76 (s, 1H), 7.98 (m, 1H), 8.35–8.40 (m, 3H). EIMS: (m/z): 328 (M^+) (Calcd. for $C_{21}H_{12}O_2S$: 328.1).

3) 6-Methyl-anthra[2,3-*b*]benzo[*d*]thiophene (Me-ABT): To an ice-cooled suspension of $LiAlH_4$ (0.455 g, 12 mmol) and $AlCl_3$ (1.6 g, 12 mmol) in dry tetrahydrofuran (100 mL) was added compound **2** (1 g, 3 mmol under a nitrogen atmosphere). The mixture was maintained for 1 h at 0 °C and then was stirred at 100 °C for another 12 h. After HCl (6 M, 50 mL) was slowly added under cooling with ice, the reaction mixture was stirred at room temperature for 30 min. The residue was filtered, washed with water, ethanol, and hexane, and further recrystallized from tetrahydrofuran, to afford 0.447 g (49.2%) of Me-ABT as a yellow solid. ^{1}H NMR (400 MHz, $CDCl_3$, δ): 2.5–2.6 (s, 3H), 7.30–7.33 (d, 1H), 7.45–7.52 (m, 2H), 7.78–7.79 (m, 2H), 7.93–7.95 (m, 1H), 8.27–8.28 (m, 1H), 8.40 (s, 1H), 8.45 (s, 1H), 8.54 (s, 1H), 8.76 (s, 1H). EIMS: (m/z): 298 (M^+) (Calcd. for $C_{21}H_{14}S$: 298.1). Anal. calcd for $C_{21}H_{14}S$: C 84.53, H 4.73; found: C 84.62, H 4.99.

Acknowledgements

Financial support from the National Natural Science Foundation of China (20825208, 60736004, 20721061, 60911130231), the National Major State Basic Research Development Program (2006CB806203, 2006CB932103, 2009CB623603), and the Chinese Academy of Sciences is kindly acknowledged. Supporting Information is available online from Wiley InterScience or from the author.

Received: September 4, 2009
Revised: December 8, 2009
Published online: March 1, 2010

[1] a) E. Menard, A. Marchenko, V. Podzorov, M. E. Gershenson, D. Fichou, J. A. Rogers, *Adv. Mater.* **2006**, *18*, 1552. b) A. L. Briseno, S. C. B. Mannsfeld, M. M. Ling, S. Liu, R. J. Tseng, C. Reese, M. E. Roberts, Y. Yang, F. Wudl, Z. N. Bao, *Nature* **2006**, *444*, 913. c) A. L. Briseno, S. C. B. Mannsfeld, S. A. Jenekhe, Z. N. Bao, Y. N. Xia, *Mater. Today* **2008**, *11*, 38.

[2] a) Q. X. Tang, L. Q. Li, Y. B. Song, Y. L. Liu, H. X. Li, W. Xu, Y. Q. Liu, W. P. Hu, D. B. Zhu, *Adv. Mater.* **2007**, *19*, 2624. b) Y. Hu, G. F. Dong, C. Liu, L. D. Wang, Y. Qiu, *Appl. Phys. Lett.* **2006**, *89*, 072108. c) R. M. Meixner, H. Göbel, F. A. Yildirim, W. Bauhofer, W. Krautschneider, *Appl. Phys. Lett.* **2006**, *89*, 092110. d) M. Debucquoy, S. Verlaak, S. Steudel, K. Myny, J. Genoe, P. Heremans, *Appl. Phys. Lett.* **2007**, *91*, 103508. e) Y.-Y. Noh, D.-Y. Kim, Y. Yoshida, K. Yase, B.-J. Jung, E. Lim, H.-K. Shim, *Appl. Phys. Lett.* **2005**, *86*, 043501. f) M. Y. Cho, S. J. Kim, Y. D. Han, D. H. Park, K. H. Kim, D. H. Choi, J. S. Joo, *Adv. Funct. Mater.* **2008**, *18*, 2905. g) T. P. I. Saragi, R. Pudzich, T. Fuhrmann-Lieker, J. Salbeck, *Appl. Phys. Lett.* **2007**, *90*, 143514. h) Y. L. Guo, C. Y. Du, C.-A. Di, J. Zheng, X. N. Sun, Y. G. Wen, L. Zhang, W. P. Wu, G. Yu, Y. Q. Liu, *Appl. Phys. Lett.* **2009**, *94*, 143303. i) B. Mukherjee, M. Mukherjee, Y. Choi, S. Pyo, *J. Phys. Chem. C* **2009**, *113*, 18870.

[3] a) A. L. Briseno, R. J. Tseng, M. M. Ling, E. H. L. Falcao, Y. Yang, F. Wudl, Z. N. Bao, *Adv. Mater.* **2006**, *18*, 2320. b) S. C. B. Mannsfeld, A. Sharei, S. H. Liu, M. E. Roberts, I. McCulloch, M. Heeney, Z. N. Bao, *Adv. Mater.* **2008**, *20*, 4044.

[4] a) K. Xiao, J. Tao, Z. W. Pan, A. A. Puretzky, I. N. Ivanov, S. J. Pennycook, D. B. Geohegan, *Angew. Chem. Int. Ed.* **2007**, *46*, 2650. b) L. Schmidt-Mende, A. Fechtenkötter, K. Müllen, E. Moons, R. H. Friend, J. D. MacKenzie, *Science* **2001**, *293*, 1119. c) S. Xiao, J. Tang, T. Beetz, X. Guo, N. Tremblay, T. Siegrist, Y. Zhu, M. Steigerwald, C. Nuckolls, *J. Am. Chem. Soc.* **2006**, *128*, 10700. d) Y. S. Zhao, H. B. Fu, F. Q. Hu, A. D. Peng, J. N. Yao, *Adv. Mater.* **2007**, *19*, 3554.

[5] a) A. Afzali, C. D. Dimitrakopoulos, T. L. Breen, *J. Am. Chem. Soc.* **2002**, *124*, 8812. b) Q. Miao, T.-Q. Nguyen, T. Someya, G. B. Blanchet, C. Nuckolls, *J. Am. Chem. Soc.* **2003**, *125*, 10284. c) D. H. Kim, D. Y. Lee, H. S. Lee, W. H. Lee, Y. H. Kim, J. I. Han, K. Cho, *Adv. Mater.* **2007**, *19*, 678.

[6] a) M. Mas-Torrent, M. Durkut, P. Hadley, X. Ribas, C. Rovira, *J. Am. Chem. Soc.* **2004**, *126*, 984. b) M. Mas-Torrent, P. Hadley, S. T. Bromley, X. Ribas, J. Tarrés, M. Mas, E. Molins, J. Veciana, C. Rovira, *J. Am. Chem. Soc.* **2004**, *126*, 8546.

[7] a) S. Subramanian, S. K. Park, S. R. Parkin, V. Podzorov, T. N. Jackson, J. E. Anthony, *J. Am. Chem. Soc.* **2008**, *130*, 2706. b) Y. Zhou, W. J. Liu, Y. G. Ma, H. L. Wang, L. M. Qi, Y. Cao, J. Wang, J. Pei, *J. Am. Chem. Soc.* **2007**, *129*, 12386. c) A. L. Briseno, S. C. B. Mannsfeld, X. Lu, Y. Xiong, S. A. Jenekhe, Z. N. Bao, Y. N. Xia, *Nano. Lett.* **2007**, *7*, 668. d) M. M. Payne, S. R. Parkin, J. E. Anthony, C.-C. Kuo, T. N. Jackson, *J. Am. Chem. Soc.* **2005**, *127*, 4986.

[8] Y. L. Guo, H. P. Zhao, G. Yu, C.-A. Di, W. Liu, S. D. Jiang, S. K. Yan, C. R. Wang, H. L. Zhang, X. N. Sun, X. T. Tao, Y. Q. Liu, *Adv. Mater.* **2008**, *20*, 4835.

[9] a) M. L. Tang, T. Okamoto, Z. N. Bao, *J. Am. Chem. Soc.* **2006**, *128*, 16002. b) F. Valiyev, W.-S. Hu, H.-Y. Chen, M.-Y. Kuo, I. Chao, Y.-T. Tao, *Chem. Mater.* **2007**, *19*, 3018. c) Y. K. Che, A. Datar, K. Balakrishnan, L. Zang, *J. Am. Chem. Soc.* **2007**, *129*, 7234. d) C. Y. Du, Y. L. Guo, Y. Q. Liu, W. F. Qiu, H. J. Zhang, X. K. Gao, Y. Liu, T. Qi, K. Lu, G. Yu, *Chem. Mater.* **2008**, *20*, 4188.

[10] J.-M. Choi, J. Lee, D. K. Hwang, J. H. Kim, S. Im, E. Kim, *Appl. Phys. Lett.* **2006**, *88*, 043508.

[11] M. C. Hamilton, S. Martin, J. Kanicki, *IEEE Trans. Electron. Devices* **2004**, *51*, 877.

[12] N. M. Johnson, A. Chiang, *Appl. Phys. Lett.* **1984**, *45*, 1102.